Biochemical Pharmacology 152 (2018) 21–33

Contents lists available at ScienceDirect

Biochemical Pharmacology

journal homepage: www.elsevier.com/locate/biochempharm

Inhibition of O-linked N-acetylglucosamine transferase activity in PC12 cells – A molecular mechanism of organophosphate flame retardants developmental neurotoxicity

Yuxin Gu[a,b], Yu Yang[a,*], Bin Wan[a,b], Minjie Li[c], Liang-Hong Guo[a,b,*]

[a] State Key Laboratory of Environmental Chemistry and Ecotoxicology, Research Center for Eco-Environmental Sciences, Chinese Academy of Sciences, P.O. Box 2871, 18 Shuangqing Road, Beijing 100085, China
[b] University of Chinese Academy of Sciences, Beijing 100049, China
[c] Institute of Process Engineering, Chinese Academy of Sciences, 1 North 2nd Street, Zhongguancun, Haidian District, Beijing 100190, China

ARTICLE INFO

Keywords:
Organophosphate flame retardants
O-linked N-acetylglucosamine transferase
Inhibition
Developmental neurotoxicity
Molecular docking

ABSTRACT

Organophosphate flame retardants (OPFRs), as alternatives of brominated flame retardants, can cause neurodevelopmental effects similar to organophosphate pesticides. However, the molecular mechanisms underlying the toxicity remain elusive. O-linked N-acetylglucosamine (O-GlcNAc) transferase (OGT) regulates numerous neural processes through the O-GlcNAcylation modification of nuclear and cytoplasmic proteins. In this study, we aimed to investigate the molecular mechanisms accounting for the developmental neurotoxicity of OPFRs by identifying potential targets of OPFRs and the attendant effects. Twelve OPFRs were evaluated for inhibition of OGT activity using an electrochemical biosensor. Their potency differed with substituent groups. The alkyl group substituted OPFRs had no inhibitory effect. Instead, the six OPFRs substituted with aromatic or chlorinated alkyl groups inhibited OGT activity significantly, with tri-m-cresyl phosphate (TCrP) being the strongest. The six OPFRs (0–100 μM exposure) also inhibited OGT activity in PC12 cells and decreased protein O-GlcNAcylation level. Inhibition of OGT by OPFRs might be involved in the subsequent toxic effects, including intracellular reactive oxygen species (ROS), calcium level, as well as cell proliferation and autophagy. Molecular docking of the OGT/OPFR complexes provided rationales for the difference in their structure-dependent inhibition potency. Our findings may provide a new biological target of OPFRs in their neurotoxicological actions, which might be a major molecular mechanism of OPFRs developmental neurotoxicity.

1. Introduction

Organophosphate flame retardants (OPFRs), as alternatives of brominated flame retardants (BFR), are widely used in various consumer products such as plastics, textiles, wood, and many others materials, particularly after the implementation of regulations phasing out the production and usage of polybrominated diphenyl ethers in many countries in recent years [1]. In 1992, the use of OPFRs globally totaled only 100,000 tons, whereas the consumption amounted to 500,000 tons in 2011 and reached 680,000 tons in 2015. Many of the OPFRs are frequently present as additives rather than chemically bonded to diverse materials, resulting in an easy release into different environmental compartments via volatilization, leaching and abrasion [2]. OPFRs have been found in various environments such as air (1.0 pg/m^3–730 mg/m^3) [3], dust (0.02 μg/g–15.1 mg/g) [4], soil (1.23 ng/g–30 μg/g) [5], waters (0.015 ng/L–87.4 μg/L) [6], sediments (1.0 ng/g–33.8 μg/g) [7], consumer products (0.15–180 mg/g) [2], and marine coastal biota (2.1 ng/g–810 μg/g) [2] and accumulated in living organisms and human blood, milk and urine [8–10].

Due to the structural similarity of OPFRs to organophosphate pesticides such as chlorpyrifos (CPF), several studies have suggested that OPFRs could cause neurotoxicity similar to organophosphate pesticides [11,12]. For example, tris (1,3-dichloro-2-propyl) phosphate (TDCPP) exhibited a concentration dependent neurotoxicity, inhibited DNA synthesis, decreased cell number and altered neurodifferentiation in PC12 cells, which is similar to CPF [11]. Previous studies have reported that acute neurotoxicity of organophosphate pesticides primarily occurs via inhibition of various forms of cholinesterase, such as acetylcholinesterase (AchE) [13]. Therefore, cholinergic markers (especially AChE activity) have been widely used as biomarkers in

* Corresponding authors at: State Key Laboratory of Environmental Chemistry and Ecotoxicology, Research Center for Eco-Environmental Sciences, Chinese Academy of Sciences, P.O. Box 2871, 18 Shuangqing Road, Beijing 100085, China.
E-mail addresses: yuyang@rcees.ac.cn (Y. Yang), LHGuo@rcees.ac.cn (L.-H. Guo).

https://doi.org/10.1016/j.bcp.2018.03.017
Received 6 February 2018; Accepted 14 March 2018
Available online 17 March 2018
0006-2952/

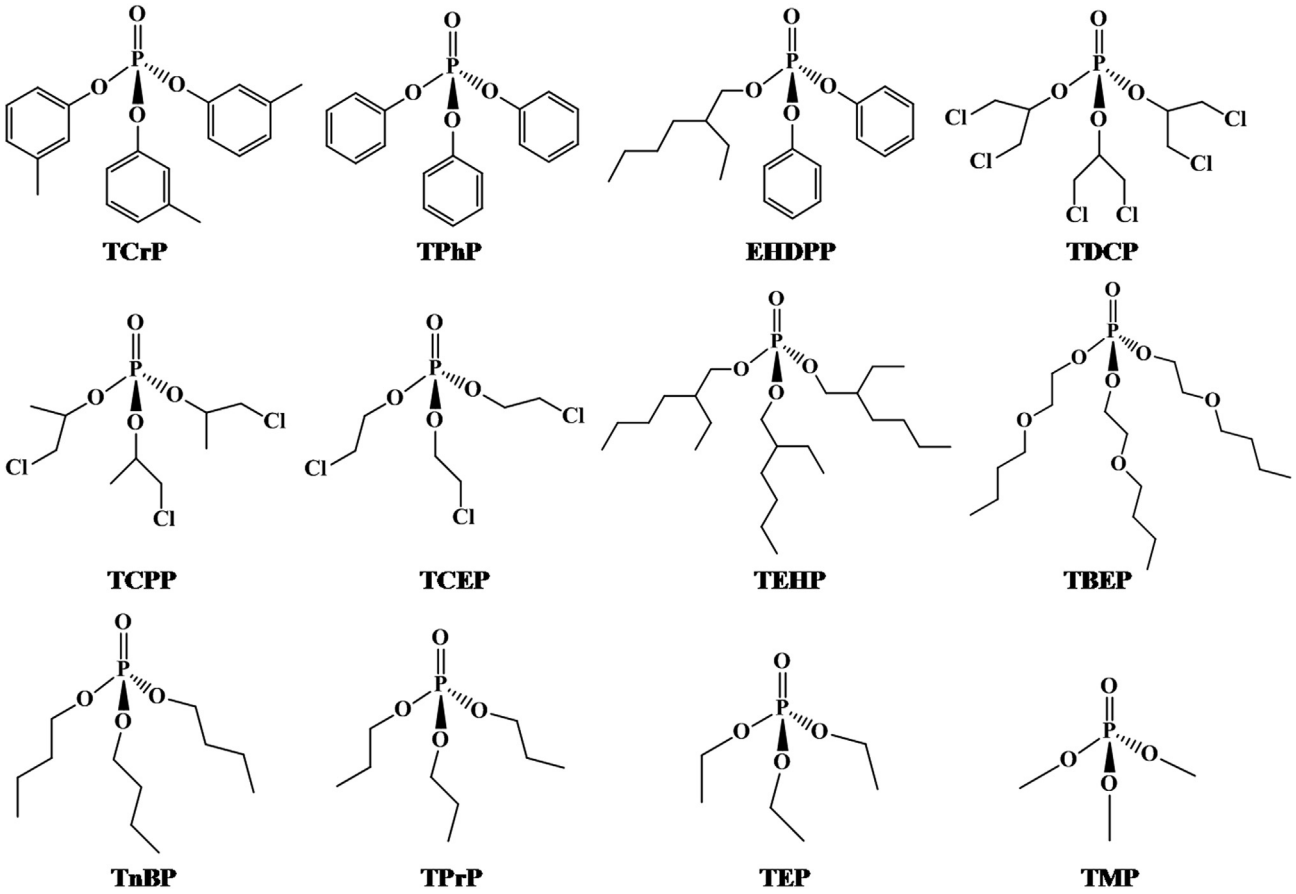

Fig. 1. Structures of OPFRs.

determining the neurotoxicity of organophosphate esters. Actually, OPFRs acts as developmental neurotoxicants. For instance, neuronal necrosis occurred in the hippocampus and thalamus of female rats by administering 350 mg/kg tris(2-chloroethyl) phosphate (TCEP) in corn oil by gavage to F344/N rats for 16 days. The cholinesterase activity was reduced by about 20% [14]. However, some studies have also reported that the mechanism of the chronic neurological toxicity of organophosphate esters cannot be solely related to cholinesterase inhibition. Organophosphate-induced delayed polyneuropathy (OPIDP) is a relatively rare neurodegenerative disorder in humans characterized by loss of function, ataxia and paralysis of distal parts of sensory and motor axons in peripheral nerves and ascending and descending tracts of spinal cord appearing 2–3 weeks after exposure or later [15]. There were thousands cases of OPIDP due to triorthocresyl phosphate (TOCP) poisoning in USA, Morocco, Italy, Romania, Srilanka, Yugoslavia and China [16]. The molecular target for OPIDP is considered to be an enzyme in the nervous system known as neuropathy target esterase (NTE) [17]. Hou et al induced OPIDP in hens using 750 mg/kg TOCP oral administration, signs of delayed neuropathy (progressive ataxia) were first observed on the 8th day post-dosing, progressing into paralysis by the 14th day for all hens. The NTE activity of brain, spinal cord, and sciatic nerve in hens was inhibited by 72%, 71% and 87% respectively. The amount of inhibited human NTE that is required before OPIDP occurs is not yet known, but appears to be less than required in the hen [18]. In addition, several non-cholinesterase targets of OPFRs have been reported. TCEP, TDCPP and triphenyl phosphate (TPhP) exhibited widespread effects on the neurotrophic factors and their receptors in Chinese rare minnow [19]. TDCPP and TCEP also decreased the expression levels of nervous system-related genes and proteins (e.g., GAP43, tubulin and NF-H) in PC12 cells [20]. Some OPFRs showed perceptible inhibitory effects on the activity of lysine decarboxylase in PC12 cells [21]. All these suggest the possibility that OPFRs may act on other biological targets and such interactions may have the relevance in mediating the OPFRs developmental neurotoxicity.

O-linked N-acetylglucosamine (O-GlcNAc) transferase (OGT) is an essential mammalian enzyme that regulates numerous cellular processes through the attachment of O-GlcNAc to serine and threonine residues of nuclear and cytoplasmic proteins [22,23]. O-GlcNAcylated proteins exist abundantly in brain, and OGT expression is enriched at neuronal synapses [24–26]. OGT has been found to dynamically modify various neuronal proteins related to synaptic function, learning and memory, and neurodegeneration [27,28]. Especially, multiple proteins involved in neurodegenerative diseases (Alzheimer's and Parkinson's disease) have been shown to be O-GlcNAcylated, including tau, amyloid precursor protein, and α-synuclein [29]. O-GlcNAc levels of a tau-enriched cytoskeletal fraction from the Alzheimer's disease (AD) brain are significantly reduced as compared to age-matched healthy controls and neurofibrillary tangles appear to completely lack O-GlcNAc [29]. Also, nucleoporin 62 (Nup62), as the known O-GlcNAcylated model protein, is extensively modified with as many as 10O-GlcNAc residues by the action of OGT. Other nuclear pore proteins are quantitatively regulated through their interaction with O-GlcNAcylated Nup62 [30]. Neuron-specific knockout of OGT in mice results in locomotor defects, increased hyperphosphorylated tau and death within 10 days of birth [31]. Forebrain-specific loss of OGT in adult mice leads to progressive neurodegeneration, including widespread neuronal cell death, neuroinflammation, increased production of hyperphosphorylated tau and amyloidogenic Aβ-peptides, and memory deficits [32]. Sensory neuron-specific knock-out of OGT in mice results in behavioral hyposensitivity to thermal and mechanical stimuli accompanied by decreased epidermal innervation and cell-body loss in the dorsal root ganglia [33]. Most importantly, human cortical brain tissue from AD patients has

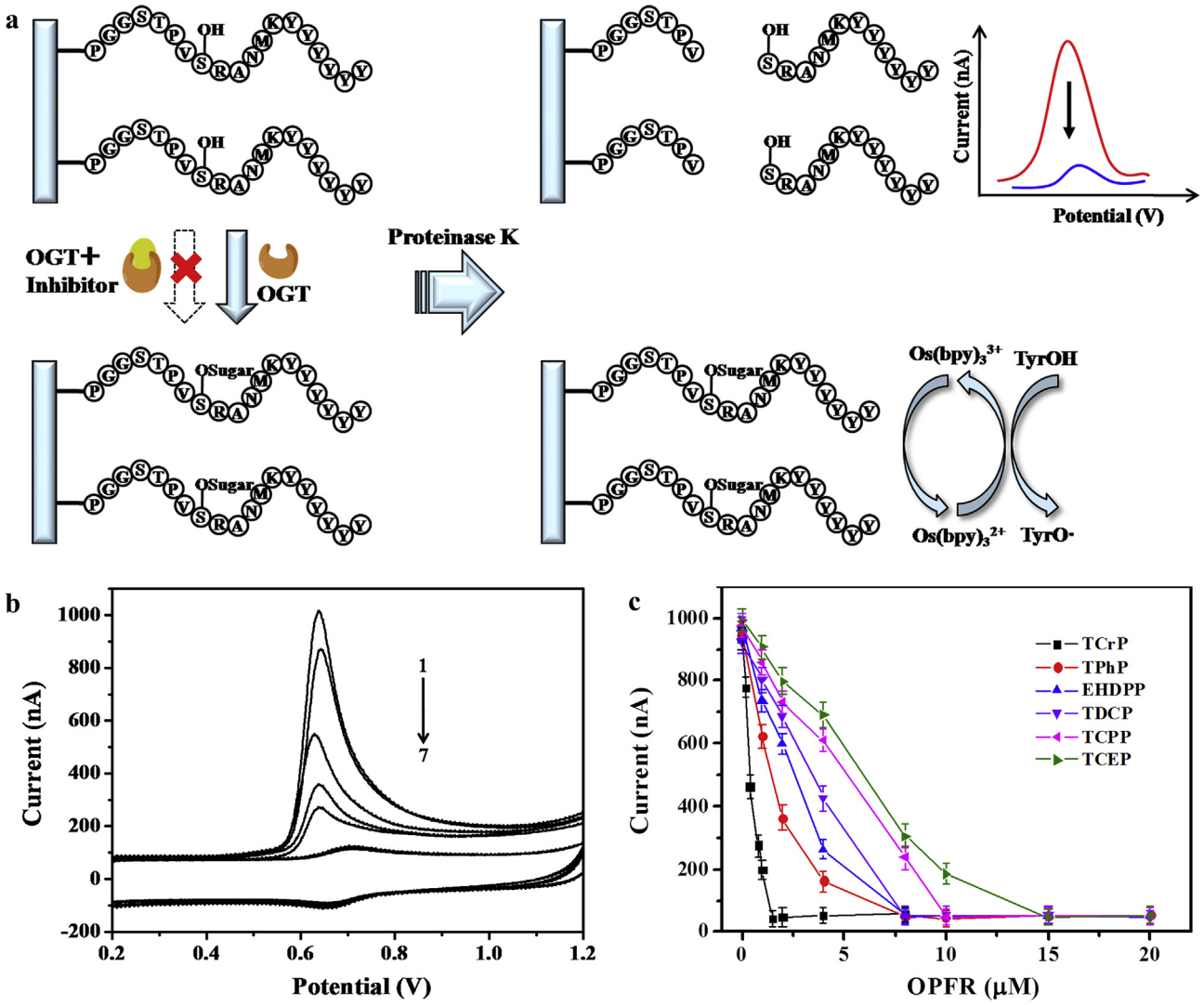

Fig. 2. (a) Design of an electrochemical biosensor for the assay of OGT activity and screening of OGT inhibitor. OGT activity produces a high current because the tyrosine-rich portion of the peptide, having become resistant to proteinase K cleavage as a result of OGT glycation, remains bound to the electrode where tyrosines are oxidized by $Os(bpy)_3^{2+}$. In the absence of OGT activity the current is low because the tyrosine-rich portion of the peptide detaches from the electrode during digestion with proteinase K. Tyrosine oxidation does not take place, and the current is low. (b) Cyclic voltammograms of the biosensor in the presence of various concentrations of TCrP at (1) 0, (2) 0.2, (3) 0.4, (4) 0.8, (5) 1, (6) 1.5, (7) 2 μM. Current is high in the absence of inhibitor (1), but is negligible when OGT activity is completely inhibited by 2 μM TCrP (7). (c) Dose-effect inhibition curves of OPFRs on OGT activity. Error bars indicate the standard deviation of three separate measurements (n = 3). Electrochemical measurements were carried out in 20 mM PB (pH 7.4) containing 3 μM $Os(bpy)_3^{2+}$. The electrode area in contact with the electrolyte was 25 mm^2. Voltage scan rate: 30 mV s^{-1}.

significantly reduced levels of OGT protein expression compared with cortical tissue from control individuals [32]. A recent study on patients with X-linked intellectual disability (XLID) found that defect in O-GlcNAc homeostasis plays an important role in mediation of XLID in individuals with OGT mutations [34]. These studies indicate that OGT regulates pathways critical for the maintenance of neuronal health and suggest that dysfunctional O-GlcNAc signaling may be an important contributor to neurodegenerative diseases.

One of the most prominent toxic effects of OPFRs on human and experimental animals is developmental neurotoxicity. Unfortunately, the molecular mechanism underlying the toxicity remains poorly understood. Considering the insufficient knowledge of OPFRs developmental neurotoxicity, and the important roles of OGT implicated in nerve system, we hypothesized that OGT might be involved in the developmental neurotoxicity of OPFRs. The main goal is the investigation of the neurotoxicological mechanisms of OPFRs by identifying new biological targets of OPFRs and the resulting toxic effects derived from their interaction. We first employed an electrochemical biosensor-based assay to screen the inhibitory effects of twelve OPFRs on OGT activity. Cellular responses to a specific hazardous chemical may reveal whether the body contains the chemical and how the toxic effects are developing. Thereafter, within cells, we further confirmed the inhibition reaction and subsequent toxic effects at environmentally relevant doses. The selected twelve OPFRs (Fig. 1), widely found in environmental media, are structurally diverse, with different substituent groups, which would allow us to investigate the relationship between OPFR structure and their inhibition potency.

2. Materials and methods

2.1. Reagents and instrumentation

Recombinant human OGT (accession #O15294) was purchased from R&D Systems Inc. OGT substrate peptide with the sequence of PGGSTPVSRANMKYYYYYY was synthesized from GL biochemical Ltd (Shanghai, China). (3-glycidoxypropyl)-trimethoxysilane (GPTMS), proteinase K, uridine 5′-diphospho-N-acetylglucosamine sodium salt (UDP-GlcNAc), alkaline phosphatase, 2′,7′-dichlorofluorescin diacetate

(DCFH-DA) and monodansylcadaverine (MDC) were bought from Sigma Aldrich (St. Louis, MO, USA). ITO conductive glass was obtained from Nanbo Corporation (Shenzhen, Guangdong, China). The metal complex $Os(bpy)_3Cl_2$ was prepared according to the procedures described elsewhere [35]. Trimethyl phosphate (TMP), triethyl phosphate (TEP), TCEP, tri-n-propyl phosphate (TPrP), tris(2-chloroisopropyl) phosphate (TCPP), tri(2-chloro-1-(chloromethyl)ethyl) phosphate (TDCP), TPhP, tri-n-butyl phosphate (TnBP), tributoxyethyl phosphate (TBEP), tri-m-cresyl phosphate (TCrP), 2-ethylhexyl diphenyl phosphate (EHDPP) and tris(2-ethylhexyl) phosphate (TEHP) were purchased from Dr. Ehrenstorfer Gmbh (Germany) (Fig. 1). Peptide was dissolved in 20 mM phosphate buffer (PB, pH 7.4). Dynabeads® M-280 tosylactivated (catalog No. 14204), fetal calf serum, horse serum, penicillin and streptomycin were purchased from Invitrogen Corporation (Carlsbad, CA, USA). Trizol reagent was from Invitrogen (CA, USA). BCA Protein Assay Kit was purchased from Beyotime Institute of Biotechnology (Shanghai, China). Protein G beads and fluo-4 NW Calcium Assay Kit were obtained from Invitrogen (Carlsbad, CA, USA). Anti-OGT antibody (ab177941) and anti-O-linked N-acetylglucosamine antibody (ab2739) were obtained from Abcam (Cambridge, UK). Cell proliferation reagent WST-1 was purchased from Roche Applied Science Inc (Penzberg, Germany). RevertAid first strand cDNA synthesis Kit was obtained from Thermo Scientific (Massachusetts, USA). GoTaq® qPCR master mix was from Promega (Fitchburg, WI, USA). Nup62 antibody was from GeneTex Inc (Irvine, CA, USA). β-actin, β-Actin (13E5) Rabbit mAb antibody (#4970) and tau (Tau46) mouse mAb antibody were purchased from Cell Signaling Technology Inc (Boston, USA). Nerve growth factor (NGF) was bought from Alomone Labs Ltd (Jerusalem, Israel). All reagents were of analytical reagent grade. Solutions were prepared in high-purity water from a Millipore milli-Q (Biocel) water purification system (Billerica, MA, USA). PCR instrument (GeneAmp®PCR System 9700), NanoDrop UV–Vis spectrophotomerter (Thermo, MA, USA), ELISA plate reader Varioskan Flash (Thermo, MA, USA), Real-time fluorescence quantitative PCR instrument Mx3005P (Stratagene, CA, USA), Vertical Electrophoresis instrument (Bio-rad, CA, USA), Confocal laser scanning microscOPFR (Leica, Wetzlar, Germany).

2.2. Electrochemical measurement of OGT inhibition by OPFRs

In the sensor, a peptide substrate with tyrosine residues at C-terminal contained a unique protease site adjacent to the glycosylation site, and was covalently immobilized on the surface of indium tin oxide (ITO) electrode by silane chemistry (Fig. 2a) [36]. $Os(bpy)_3^{2+}$-mediated tyrosine oxidation current was used as the signal reporter. When the O-GlcNAcylation was achieved, the glycosylated peptides could not be cleaved by proteinase K and resulted in a high current response on ITO electrode. However, when the O-GlcNAcylation was successfully inhibited using a small molecule, the unglycosylated peptides could be cleaved easily and led to low current signal (Fig. 2a). The resulting electro-catalyzed oxidation signal of tyrosine was measured, which was associated with the OGT activity [36]. OGT activity assay was performed according to the following procedure. Firstly, the reaction mixture containing 25 mM Tris-HCl (pH 7.4), 10 mM $CaCl_2$, 0.05% Tween-20, 0.05% NP-40, 50 μM UDP-GlcNAc, 0.1 U mL^{-1} alkaline phosphatase and OGT in a total volume of 10 μL was deposited onto the surface of the peptide-modified electrode and incubated in a moisturized container at 37 °C for 45 min. UDP is a potent inhibitor of OGT activity. Alkaline phosphatase converts UDP to UMP, which is not an inhibitor of OGT. For the inhibition experiment, varying concentration of inhibitor was included in the reaction mixture of OGT. Then, the proteinase K solution containing 10 mM Tris-HCl (pH 7.4), 1 mM Ca $(CH_3COO)_2$ was coated onto the surface of the electrode and incubated in a moisturized container at 37 °C for 60 min. After washing in PB, cyclic voltammograms (CVs) were measured in 3 μM $Os(bpy)_3^{2+}$/20 mM PB (pH 7.4). Moreover, an IC_{50} value, half-maximal inhibition, could be estimated from the dose-effect curve [37]. Electrochemical measurements were carried out on a CHI 660B electrochemistry analyzer from CH Instruments (Austin, TX) with an ITO work electrode, a Pt counter electrode and an Ag/AgCl reference electrode.

2.3. Cell culture, treatment and viability test

Pheochromocytoma PC12 cells, a cell line derived from rat adrenal medulla, were obtained from ATCC (Manassas, VA, USA), and maintained in Dulbecco's modified Eagle's medium supplemented with 6% fetal calf serum, 6% horse serum, 100 units mL^{-1} penicillin and 100 μg mL^{-1} streptomycin in a humidified CO_2 incubator at 37 °C. Approximated 0.5–1 × 10^5 cells mL^{-1} in 96-well plates was seeded for cell viability assay. The exposure was performed in DMEM with or without (DMSO control) OPFRs (up to 250 μM), respectively. The change of cell viability after 24 h OPFRs exposure was determined by cell proliferation reagent WST-1. In brief, after the exposure, WST-1 reagents (1:10 dilution) were added into each well of the 96-plate, and then incubated at 37 °C for 4 h. The absorbances were recorded on a Varioskan Flash microplate reader at 440 nm, and the absorbance at 600 nm was used as reference.

2.4. Total RNA isolation and gene expression analysis

The PC12 cells were seeded in 60 mm × 60 mm dish and cultured for 12 h. Cells were stimulated with nerve growth factor (NGF) (50 ng mL^{-1}, 5 days) and then exposed to OPFRs (0–100 μM) or control medium (VC) for 24 h. Total RNA was extracted from cells exposed to OPFRs using Trizol reagent. The quality and quantity of the purified total RNA were assessed by Nanodrop 1000 spectrophotometer. The gene expression of OGT (UniProt accession number: P56558) was analyzed by using real-time reverse-transcriptase polymerase chain reaction (RT-PCR). First, total RNA was converted to first-strand cDNA with reverse transcription using oligo(dT)18 primer. Quantitative PCR (QPCR) was then performed using the GoTaq® qPCR Master Mix Kit. The assay was performed in triplicates on a Mx3005P real-time QPCR system. The sequences of PCR primers used were as follows: OGT Left: 5′-CCA GCA GTA GGA GAG CCC AAT-3′; Right: 5′-CCC AGA GAA CAT CCA TCC CT-3′; β-actin Left: 5′-TTG CCC TAG ACT TCG AGC AA-3′; Right: 5′-CAG GAA GGA AGG CTG GAA GA-3′. PCR reaction was performed as follows: 2 min at 95 °C followed by 30 s at 95 °C, 30 s at 60 °C for 40 cycles. The cycle threshold (Ct) for each sample was generated automatically by the MxPro software (Strategene, La Jolla, CA, USA). The Ct value for each sample corresponds to the point at which the fluorescence crosses the threshold. After PCR, melting curve analysis was performed and the PCR products were visualized using gel electrophoresis to assess the specificity of PCR amplification reactions. The house keeping gene, β-actin (UniProt accession number: P60711) was used as an endogenous control. The ratio of gene expression between control and treatment groups was calculated by using the 2-ΔΔCT method.

2.5. Western blot assay

After treatment, cell lysates (for detection of OGT, β-actin) were separated by gradient separation gel (4–20%) and 10% separation gel, respectively. The samples were transferred to polyvinylidene difluoride (PVDF) membrane (Immobilon-P, Millipore, Germany) and the membranes were blocked with 5% nonfat milk and washed three times with tris buffered saline tween 20 (TBST) (containing 0.1% Tween 20). Thereafter, the membranes were incubated with primary antibodies (1:1000 dilution) against OGT and β-actin at 4 °C for overnight, and then washed with TBST again. The membranes were incubated with corresponding HRP-conjugated secondary antibody (1:10000 dilutions) for 1 h at room temperature, followed by three washes with TBST. The target proteins were observed using an ECL kit (Merck, Germany) and

detected on X-ray film. Quantitative analysis of the band intensities was performed using Gel-pro image software (Media Cybernetics, USA). Specifically, for protein Tau or Nup62 (OGT substrate) O-GlcNAcylation analysis, protein Tau or Nup62 was collected from cell lysates by immunoprecipitation. The samples were separated by SDS-PAGE and then transferred to a PVDF membrane, followed by incubation with anti-O-linked N-acetylglucosamine primary antibody (1:1000 dilution) at 4 °C overnight and secondary antibody (1:10000 dilutions) for 1 h at room temperature. Thereafter, the membrane was regenerated for 30 min by stripping buffer, and then incubated with Nup62 antibody or Tau (Tau46) mouse mAb antibody (1:1000 dilution) at 4 °C overnight and secondary antibody (1:10000 dilutions) for 1 h at room temperature.

2.6. Immunoprecipitation

The exposed cells were lysed with RIPA lysis buffer and the protein concentration of each sample was determined by BCA Protein Assay Kit. 30 μL protein G beads and 2 μL antibody (1 μg μL^{-1}) were added to samples (500 μg μL^{-1}) and incubated for 4 h at 4 °C. The supernatant was taken out and 1 mL Tris-HCl (50 mM) was added to wash protein G beads three times. Then 30 μL loading buffer was added and boiled in an electric-heated thermostatic water bath for 5 min at 95 °C. The supernatant was obtained to use for the Western-blot detection.

2.7. OGT activity assay and global O-GlcNAcylation level in cells

For OGT activity analysis, PC12 cell lysates were collected in RIPA lysis buffer and the OGT activity was measured using high-performance liquid chromatography (HPLC) [38]. In brief, OGT immunoprecipitate was prepared from cell lysate using anti-OGT antibody conjugated dynabeads for 6 h at 4 °C. After washing away unbound lysate, reaction mixtures containing 100 μM CKII peptide (KKKYPGGSTPVSSANMM), 0.5 mM UDP-GlcNAc, 6 mM $MgCl_2$, 150 mM NaCl, 1 mM EDTA, 2.5 mM tris(hydroxypropyl)phosphine, 1 U mL^{-1} alkaline phosphatase, 20 mM Tris-HCl (pH 7.4), were added and the reaction mixture was incubated for 60 min at 37 °C with continuous shaking at 700 rpm. After being quenched by adding an equal volume of methanol, the reaction mixtures were centrifuged at 12,000*g* for 30 min. The supernatants (50 μL) were loaded onto an Agilent HPLC system to quantify the yield based on the integrated areas of glycopeptide product and peptide substrate. Thereafter, global O-GlcNAcylation level in cells was detected. In brief, PC12 cells were seeded in 60 mm × 60 mm dish and cultured for 12 h. Cells were stimulated with nerve growth factor (NGF) (50 ng mL^{-1}, 5 days) and then exposed to OPFRs (0–100 μM) or control medium (VC) for 24 h. The exposed cells were lysed with RIPA lysis buffer. The protein concentration of each sample was determined by BCA Protein Assay Kit. The samples were separated by SDS-PAGE gel electrophoresis and then transferred to a PVDF membrane (0.45 μm). The membranes were blocked in 5% nonfat milk and washed in TBST (containing 0.1% Tween 20), followed by incubation with anti-O-GlcNAc primary antibody (1:1000 dilution) at 4 °C overnight. The corresponding HRP-conjugated secondary antibody (1:10000 dilutions) was incubated with the membranes for 1 h at room temperature, followed by TBST wash. The last step was X-ray film exposure.

2.8. Determination of calcium ion level

Cells were seeded at approximated 3.0×10^4 cells/well in 96-well plates for 24 h and then exposed to OGT inhibitor alloxan (5 mM), TCrP (0–100 μM), alloxan and TCrP (0–100 μM) or control medium (VC) for different time (0–24 h). Appropriate amount of Fluo-4-AM (Ca^{2+} fluorescent probe) and 100 μL propanesulfonic acid (250 mM) were added to 10 mL NC buffer. The 100 μL probe solution were added into each well of the plate, and then incubated at 37 °C for 30 min. The excitation wavelength was set at 485 nm and the emission intensities were recorded at 535 nm on a Varioskan Flash microplate reader.

2.9. Detection of reactive oxygen species (ROS)

Cells were seeded at approximated 1.5×10^5 cells/well in 24-well plates for 24 h and then exposed to OGT inhibitor alloxan (5 mM), TCrP (0–100 μM), alloxan and TCrP (0–100 μM) or control medium (VC) for different time (0–24 h). After the exposure, 400 μL DCFH-DA (10 μM) probes were added into each well of the plate, and then incubated at 37 °C for 20 min. The excitation wavelength was set at 485 nm and the emission intensities were recorded at 535 nm on a Varioskan Flash microplate reader.

2.10. Cell proliferation assay

Cells were seeded at approximated $1–2 \times 10^4$ cells/well in 96-well plates for 12 h and then exposed to OGT inhibitor alloxan (5 mM), TCrP (0–100 μM), alloxan and TCrP (0–100 μM) or control medium (VC) for 24 h. After the exposure, WST-1 reagents (1:10 dilution) were added into each well of the plate, and then incubated at 37 °C for 2 h. The absorbances were recorded on a Varioskan Flash microplate reader at 450 nm and 690 nm.

2.11. Cell autophagy assay

Cells were seeded at approximated 2×10^4 cells/well in 8-well plates for 24 h and then exposed to OGT inhibitor alloxan (5 mM), TCrP (0–100 μM), alloxan and TCrP (0–100 μM) or control medium (VC) for 24 h. 500 μL MDC (50 μM) staining solution was added into each well of the plate, and then incubated at 37 °C for 15 min. MDC is a selective marker for autophagic vacuoles. Intracellular vacuoles can be labeled by MDC *in vivo*, and then measured by a laser scanning confocal microscOPFR.

2.12. Molecular docking

Molecular docking was performed using Autodock Vina v1.1.2 (San Francisco, CA, USA). Briefly, small molecule structures were built by Discovery Studio Visuilazier 4.5 (San Diego, CA, USA) and optimized with MOPAC program [39]. The optimized small molecules were docked with the OGT model using Autodock Vina. Polar hydrogens as well as Kollman United charges were added by AutoDockTools. The obtained ligand-protein complex was further analyzed by MD simulation using GROMACS program [40] to obtain binding energy of complex.

2.13. Statistical analysis

Results are expressed as mean ± SD (n = 4, SD means the standard deviation of four measurements). The statistical analysis was performed using SPSS statistics software (Chicago, IL). The normality and homogeneity of variance of all data were analyzed by one-way analysis of variance (ANOVA) and then the multiple comparisons for differences in means were performed by Bonferroni's post hoc test. A p-value < 0.05 was considered statistically significant.

3. Results

3.1. Inhibition of OGT activity by OPFRs using an electrochemical enzyme assay

Based on our established method, an electrochemical biosensor for the assay of the OGT enzyme activity was employed [36]. The sensing mechanism was based on the combination a protease-protection strategy with electrocatalytic oxidation of tyrosine mediated by osmium bipyridine (Fig. 2a). Twelve OPFRs with different substitution groups were screened for their inhibitory effects on OGT activity, which include six alkyl chains (TMP, TEP, TPrP, TnBP, TBEP and TEHP), three

Table 1
IC_{50} for inhibition of human OGT activity determined by electrochemical detection of tyrosine oxidation and some molecular docking results of OPFRs.

OPFRs name	Abbreviation	IC_{50} (μM)	Hydrogen bonds	Electrostatic interaction	Binding energy (Kcal/M)
Tri-*m*-cresyl phosphate	TCrP	0.50	Thr922	Asp925	−7.60
Triphenyl phosphate	TPhP	1.80	–	Asp925	−7.10
2-Ethylhexyl diphenyl phosphate	EHDPP	2.90	–	Asp925	−6.60
Tri(2-chloro-1-(chloromethyl)ethyl) phosphate	TDCP	4.00	His901	Asp925	−5.50
Tris(2-chloroisopropyl)phosphate	TCPP	5.20	His901	Asp925	−5.00
Tri(2-chloroethyl) phosphate	TCEP	6.10	His901	Asp925	−4.80
Tri-*n*-butyl phosphate	TnBP	ND	His920, Thr921, Thr922	–	−2.5
Tri-*n*-propyl phosphate	TPrP	ND	His920, Thr921, Thr922	–	−2.4
Triethyl phosphate	TEP	ND	His920, Thr921, Thr922	–	−2.4
Tris(2-ethylhexyl) phosphate	TEHP	ND	Lys842, His920, Thr921, Thr922	–	−1.5
Tributoxyethyl phosphate	TBEP	ND	Lys842, His920, Thr921, Thr922	–	−1.5
Trimethyl phosphate	TMP	ND	Lys842, His920, Thr921, Thr922	–	−1.2

ND: not detected.

chlorinated alkyl chains (TCEP, TCPP and TDCP), and three aromatic groups (TPhP, TCrP and EHDPP). As shown in Fig. 2b and c, remarkable inhibitory effect was observed for the six OPFRs substituted with chlorinated alkyl chains or aromatic groups. By comparison, the other six OPFRs substituted with alkyl chains did not show any effect on the activity of OGT. According to the dose-effect curves, the IC_{50} values were obtained (Table 1). Their inhibition potency differed significantly, which was closely associated with the type of substituents. The OPFRs substituted with aromatic groups showed stronger inhibition potency than those substituted with chlorinated alkyl chains. The inhibitory effect follows the order of TCrP > TPhP > EHDPP > TDCP > TCPP > TCEP. Among them, TCrP, an OPFR substituted with cresyl, showed the strongest inhibitory effect on the activity of OGT with an IC_{50} of 0.50 μM.

3.2. Inhibition of OGT activity by OPFRs in PC12 cells

Due to high expression of OGT, PC12 cells were used to further investigate the effect of these six OPFRs on OGT activity in biological systems. Also, OPFRs are detected at high concentrations in residential dust, indoor air and consumer products (e.g. acoustic ceiling coatings and PUF fillers) and bioaccumulated in the organisms. Therefore, cell experiment assays were performed in the high concentration range of OPFRs. In order to obtain non-cytotoxic concentrations, WST-1 assay was employed to detect the cell viability of PC12 cells after 24 h exposure to OPFRs (0–250 μM) (Fig. 3). We found that cell viability significantly decreased when exposed to 100 μM EHDPP, 120 μM TPhP, 140 μM TDCP or 160 μM TCrP, respectively, whereas it did not change appreciably after TCEP or TCPP exposure. Then, OGT activity was measured in cells under the exposure of non-cytotoxic concentrations of TCrP, TPhP, TDCP, TCEP, TCPP (0–100 μM), EHDPP (0–50 μM) or control medium (VC). This allowed us to ensure that changes in OGT activity were due to OPFR treatment but not a secondary effect of cell death. OGT was immuno-precipitated from the cell lysates, and its activity was measured by the addition of a CKII peptide substrate and diphosphonucleotide sugars as donor substrates, and quantification of the yield based on the integrated areas of glycopeptide product and peptide substrate. As shown in Fig. 4a-f, the six OPFRs were all found to inhibit OGT activity in a concentration-dependent manner in living cells. At 50 μM exposure, TCrP, TPhP, EHDPP and TDCP inhibited the OGT activity in PC12 cells by 46%, 36%, 39%, and 41% respectively. At 100 μM exposure, TCPP and TCEP could inhibit the OGT activity by 33% and 30% respectively. The inhibition potency of aromatic group substituted OPFR, TCrP, is the strongest, which is in accordance with the results obtained from the electrochemical biosensor.

In cells, the enzymatic activity of a protein relies upon both total content and specific activity of the protein, we need to determine gene expression and protein levels of OGT in PC12 cells after OPFRs exposure. The results of RT-PCR show that TPhP, EHDPP, and TCEP increased the gene expression of OGT in a concentration-dependent manner, while no significant effect was observed after exposure to one of other three OPFRs (TCrP, TDCP and TCPP) (Fig. 5). The OGT protein level in the exposed cells was quantified using Western-blot assay (Fig. 5). Even at 25 μM exposure, TCrP and TPhP increased the protein level by 1.15 folds and 1.23 folds respectively. At 50 μM exposure, TDCP and TCPP stimulated increase of OGT protein level by 1.24 folds and 1.30 folds respectively. No significant change was shown after EHDPP or TCEP exposure. The results indicate that OGT inhibition in PC12 cells by the six OPFRs was attributed to the loss of enzyme activity, not protein content.

3.3. Change of protein O-GlcNAcylation level after OPFRs exposure

Since OGT is responsible for the modification of protein O-GlcNAcylation, its inhibition by OPFRs should lead to a decrease of O-GlcNAcylation level. We determined the global O-GlcNAcylation level first. Compared with the cells treated with culture medium, OPFRs treated cells had a significant dose-dependent decrease in the global O-GlcNAcylation level, manifested as the lower signal intensity of the treatment lanes (Fig. 4). 50 μM OPFRs exposure reduced the global O-GlcNAcylation level by 19% (TCrP), 24% (TPhP), 40% (EHDPP) and 55% (TDCP) respectively. At 100 μM exposure, TCEP and TCPP led to the decrease of 32% and 18% respectively. Then, we selected Nup62 and tau, two representative physiological substrates of OGT, to investigate the effect of OPFR inhibition on protein O-GlcNAcylation level in cells. After exposure to one of the six OPFRs, PC12 cells were lysed and the levels of both protein and O-GlcNAcylated protein were detected by immunoblotting. Compared with the cells treated with culture medium, OPFRs treated cells had a significant dose-related decrease in the relative content of O-GlcNAcylated protein. For Nup62 (Table 2), at 50 μM exposure, TCrP, TPhP, EHDPP and TCEP reduced its O-GlcNAcylation level by 23%, 24%, 20% and 35% respectively. At 100 μM exposure, TDCP and TCPP lowered the O-GlcNAcylation level by 37% and 21% respectively. While, for tau (Table 2), at 25 μM exposure, EHDPP significantly decreased the O-GlcNAcylation level by 35% respectively. At 50 μM exposure, TPhP, EHDPP, TDCP, and TCEP lowered the O-GlcNAcylation level by 32%, 53%, 16% and 27% respectively. At 100 μM exposure, TCrP and TCPP resulted in the decrease of 30% and 32% respectively.

3.4. Ca^{2+} influx ($[Ca^{2+}]_i$) in exposed cells

Calcium has a central role as the mediator of the intracellular information flow in virtually all forms of neuroadaptation. We thus determined $[Ca^{2+}]_i$ in PC12 cells. In order to ascertain whether inhibition of OGT activity is responsible for calcium ion influx or not, alloxan, a well-known OGT inhibitor, was introduced. As shown in Fig. 6a, compared with the cells treated with culture medium, alloxan treated cells

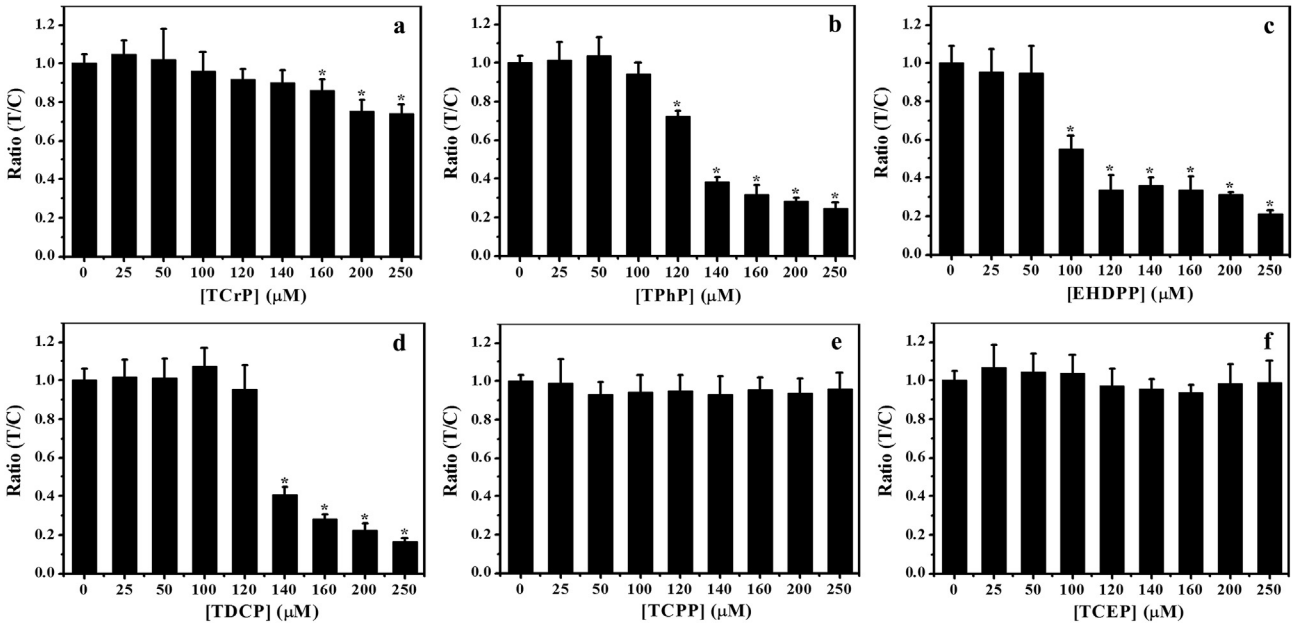

Fig. 3. Cell viability assays of PC12 cells after 24 h exposure to OPFRs respectively. T/C means treated/control. Data represent the mean ± SD of four individual experiments. Significance was set as $^{*}p < 0.05$.

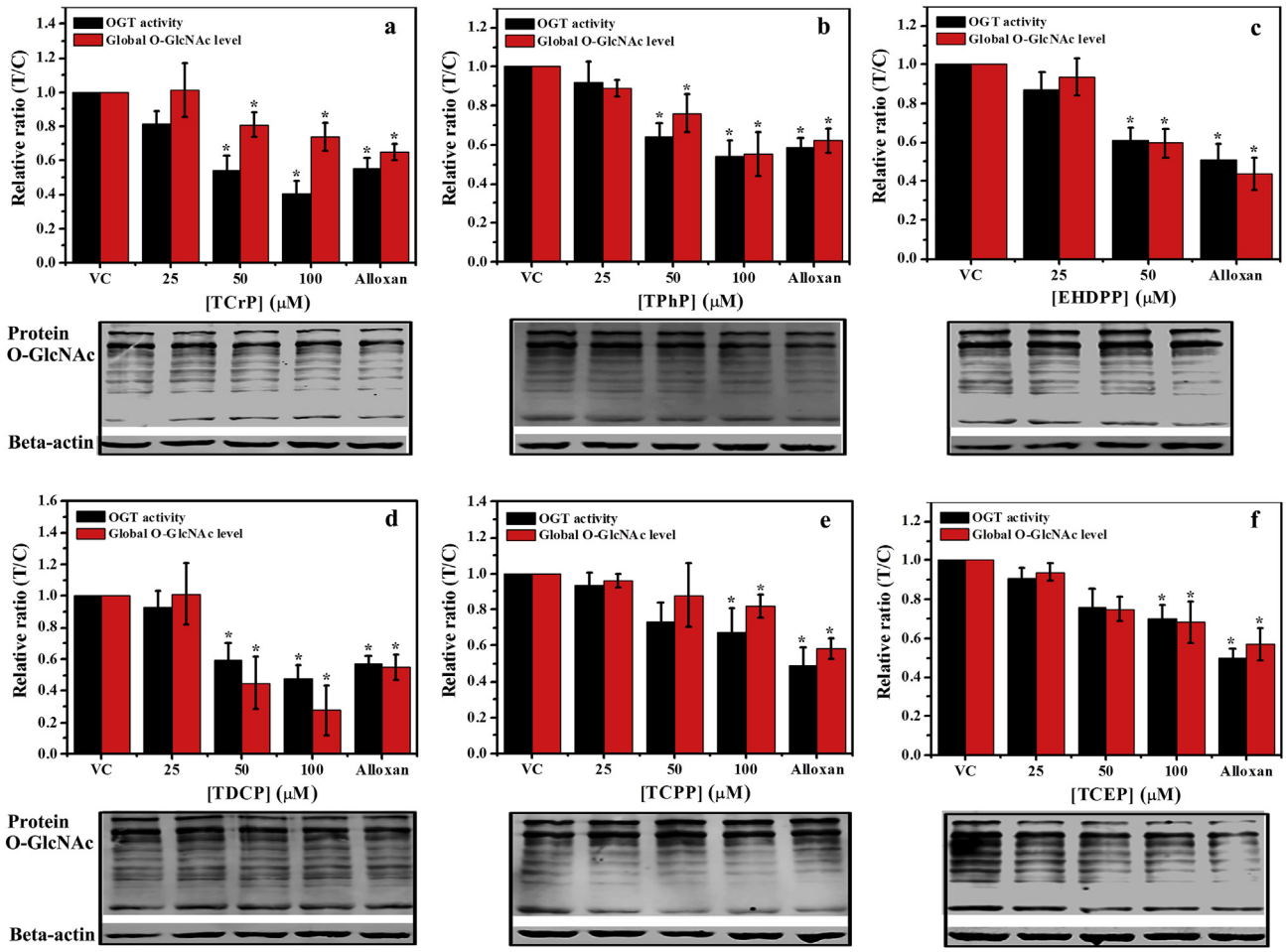

Fig. 4. OGT activity and global O-GlcNAc levels, representative images of Western-blot analysis on OGT level in PC12 cells exposed to OPFRs for 24 h. PC12 cells treated with alloxan (5 mM, 24 h) were used as positive control. T/C means treated/control. The band of global protein O-GlcNAc are in the range of 48–200KD. Data are presented as the means of four replicates and normalized against β-actin. Significance was set as $^{*}p < 0.05$.

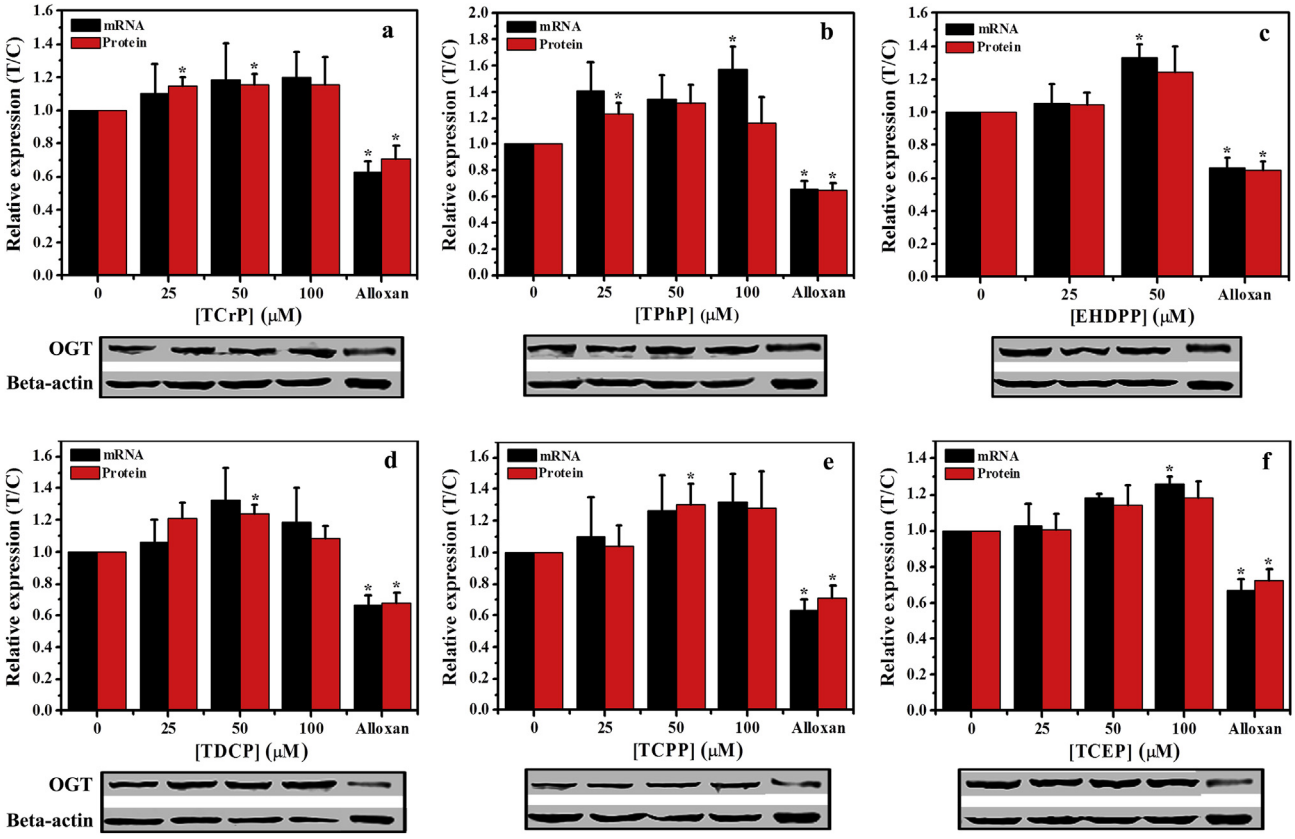

Fig. 5. Relative expression of OGT at transcriptional and protein levels, representative images of Western-blot analysis on OGT level in PC12 cells exposed to OPFRs for 24 h. PC12 cells treated with alloxan (5 mM, 24 h) were used as positive control. The molecular weight of OGT is 110KD. Data are presented as the means of four replicates and normalized against β-actin. Error bars represent SD. $^{*}p < 0.05$, compared with the control group (T/C).

induced a little increase of fluorescence intensity of Fluo-4 AM, indicating that OGT inhibition was capable of inducing calcium ion influx, which led to elevated $[Ca^{2+}]_i$. While, in alloxan and TCrP coexposed cells, elevation of $[Ca^{2+}]_i$ was significantly enhanced with the increase of TCrP concentration and then reached a plateau at 25 μM, compared to that in normal, alloxan or TCrP treated cells, indicating the pivotal role of TCrP in inducing Ca^{2+} influx.

3.5. ROS in exposed cells

ROS are chemically reactive molecules that have essential functions in living organisms. Maintaining ROS homeostasis is crucial for normal cell growth and survival. Then, we determined ROS produced in cells. Similarly, in order to explain whether inhibition of OGT activity contributed to ROS generation or not, we used OGT inhibitor-alloxan exposure to cells. As shown in Fig. 6b, compared with the cells treated with culture medium, alloxan treated cells induced a remarkable increase of ROS amounts. While, in alloxan and TCrP coexposed cells, the productions of ROS amounts were further increased with the increase of TCrP concentration and then reached a maximum at 25 μM.

3.6. Cell proliferation in exposed cells

Cell proliferation, as one of the most important biological function, is the basis of cell growth, development, reproduction and heredity in living organisms. We investigated the change of cell proliferation after exposure to OGT inhibitors. As shown in Fig. 6c, compared with the cells treated with culture medium, alloxan or OPFRs treated cells resulted in a decrease of cell proliferation. While, in alloxan and TCrP coexposed cells, cell proliferation was further markedly depressed with the increase of TCrP concentration.

3.7. Cell autophagy in exposed cells

Autophagy plays a significant role in maintaining cellular homeostasis and protects cells from varying insults, including misfolded and aggregated proteins and damaged organelles, which is particularly crucial in neuronal survival. Also, autophagy plays a key role in maintaining homeostasis of axon terminal and preventing axonal degeneration. After exposed to different OGT inhibitors, the cells were stained by MDC and then the fluorescence intensity of intracellular MDC-labeled vacuoles was detected by confocal laser scanning microscopy. As shown in Fig. 6d-n, compared with the cells treated with culture medium, alloxan treated cells resulted in an increase of fluorescence intensity. It indicated the OGT inhibition could induce the formation of the autophagic vacuoles, which led to the increase of MDC accumulation in vacuoles. While, in alloxan and TCrP coexposed cells, cell autophagy was further distinctly enhanced with the increase of TCrP concentration and then reached an invariant state at 25 μM, which suggested the evident role of TCrP in inducing cell autophagy.

3.8. Molecular docking of OPFR/OGT complexes

To better understand the inhibitory effect of OPFRs on OGT activity, the binding interaction of OPFRs with the protein was simulated by molecular docking. Previous X-ray crystal structure shows that the protein comprises three distinct regions: an amino (N)-terminal region (N-Cat) consisting of a series of tetratricopeptide repeat (TPR) units, a C-terminal domain (C-Cat) and an intervening domain (Int-D) [41]. The N-Cat and C-Cat domains have Rossmannlike folds typical of GT-B superfamily members. The Int-D domain, which has a novel fold, packs exclusively against the C-Cat domain. The residues in the active site of OGT contain Lys842, His901, His920, Thr921, and Asp925 etc.

Table 2
The O-GlcNAcylation level change of Nup62 and Tau in cells exposed to OPFRs for 24 h. PC12 cells treated with alloxan (5 mM, 24 h) were used as positive control. The molecular weights of Nup62 O-GlcNAc and Tau O-GlcNAc are about 62KD and 55KD respectively. Data represent the mean ± SD. Significance was set as $^{*}p < 0.05$.

OPFRs (μM)		Nup62 O-GlcNAc/Nup62 (T/C)	Tau O-GlcNAc/Tau (T/C)
TCrP	0	1	1
	25	0.82 ± 0.04	0.77 ± 0.19
	50	0.77 ± 0.06 (*)	0.76 ± 0.14
	100	0.75 ± 0.05 (*)	0.70 ± 0.06 (*)
	Alloxan	0.66 ± 0.02 (*)	0.69 ± 0.08 (*)
TPhP	0	1	1
	25	0.86 ± 0.04	0.83 ± 0.10
	50	0.76 ± 0.07 (*)	0.68 ± 0.12 (*)
	100	0.62 ± 0.12 (*)	0.63 ± 0.05 (*)
	Alloxan	0.63 ± 0.08 (*)	0.70 ± 0.08 (*)
EHDPP	0	1	1
	25	0.93 ± 0.15	0.65 ± 0.18 (*)
	50	0.80 ± 0.02 (*)	0.47 ± 0.13 (*)
	Alloxan	0.67 ± 0.06 (*)	0.68 ± 0.09 (*)
TDCP	0	1	1
	25	0.99 ± 0.19	0.82 ± 0.06
	50	0.81 ± 0.11	0.84 ± 0.09 (*)
	100	0.63 ± 0.07 (*)	0.76 ± 0.08 (*)
	Alloxan	0.65 ± 0.02 (*)	0.66 ± 0.03 (*)
TCPP	0	1	1
	25	0.88 ± 0.14	0.87 ± 0.15
	50	0.82 ± 0.16	0.78 ± 0.07
	100	0.79 ± 0.03 (*)	0.68 ± 0.08 (*)
	Alloxan	0.68 ± 0.07 (*)	0.76 ± 0.05 (*)
TCEP	0	1	1
	25	0.98 ± 0.13	0.83 ± 0.12
	50	0.65 ± 0.08 (*)	0.73 ± 0.10 (*)
	100	0.57 ± 0.10 (*)	0.66 ± 0.05 (*)
	Alloxan	0.66 ± 0.09 (*)	0.64 ± 0.09 (*)

Using the software of Discovery Studio, twelve OPFRs were docked into the binding pocket of OGT respectively. The binding energy and some non-covalent bond interactions obtained from the docking analysis are listed in Table 1. In the docked complexes, all the OPFRs tended to bind to the active site of OGT, which would hinder the binding of substrate to OGT. The structures of the docked complexes between OGT and one of three different OPFRs types (e.g. TCrP, TDCP or TnBP) are shown in Fig. 7. The six OPFRs substituted with chlorinated alkyl chains or aromatic groups all bond in a hydrophobic pocket formed by the residues of Phe 868, Leu866, His901, Asp925, Thr922, Pro559 and Lys842 of OGT in the C-Cat domain near the interface with the N-Cat domain (Fig. 7a-d). Especially, there was a same electrostatic interaction between the phosphorus atom of an OPFR and the carboxyl oxygen atom of Asp925 residue of OGT (Fig. 7a and c). Except for this, the exact binding geometries were strikingly different. For the three OPFRs substituted with aromatic groups, one hydrogen bond existed between the phosphate oxygen of TCrP and the carboxyl hydrogen atom of Thr922 residue of OGT (Fig. 7a and b). No hydrogen bonds existed between the phosphate oxygen of TPhP (or EHDPP) and the side chain residues of OGT (Table 1). While, for the other three OPFRs substituted with chlorinated alkyl chains, there has one different hydrogen bond formed between the phosphate oxygen of an OPFR and the imino hydrogen atom of His901 residue of OGT (Fig. 7c, d, and Table 1). A π-cation interaction existed between the phosphorus atom of an OPFR and the face of an electron-rich π system (i.e. imidazole ring of His901 residue of OGT) (Fig. 7c). Besides, there were some other non-covalent bonds, such as Van der Waals forces, π-π stacked interaction, π-alkyl interaction etc (Fig. 7a nd c), which coordinately contributed to the combination between OPFR and OGT. By comparison, for the six OPFRs substituted with alkyl chains (TEHP, TBEP, TnBP, TPrP, TEP and TMP, none is OGT inhibitor), completely different binding geometries were obtained. Several hydrogen bonds existed between the phosphate oxygen of OPFRs and the amino or carboxyl hydrogen atom of Lys842, His920, Thr921 and Thr922 of OGT (Table 1, Fig. 7e and f). Notably, an unfavorable positive-positive interaction always existed between the nitrogen atom of Lys842 residue of OGT and the phosphorus atom of an OPFR (See dotted red lines in Fig. 7e and f), which suggested that the six OPFRs could not bind well with OGT. It may provide a clue why the six alkyl substituted OPFRs did not inhibit OGT activity. Overall, our results reveal that except for the six alkyl group substituted OPFRs, the other six OPFRs bind with OGT through noncovalent interaction rather than covalent binding, which is similar to the other well-known OGT inhibitors, such as alloxan, UDP-S-GlcNAc etc [42].

4. Discussion

OGT has the highest level of expression in brain and neurons. And the level of OGT activity is ten-fold higher in brain than peripheral tissues. OGT is directly involved in regulation of neuronal development, synaptic transmission, and synaptic plasticity. The inhibition of OGT could in principle lead to the dysfunction of nerve system. It also may provide a new clue to the toxic and pathogenic effects of OPFRs. In our work, a series of experiments were performed in an attempt to establish OGT as a potential target (or biomarker) of OPFRs in neuro cells in their neurotoxic action.

In the *in vitro* OGT enzyme activity assay, we found that only the six OPFRs substituted with aromatic group or chlorinated alkyl chains inhibited OGT activity. Their inhibition potency was strongly dependent on substituent groups. By comparing OPFRs with different groups, it is clear that aromatic group substituted OPFRs are more potent than chlorinated alkyl chains substituted ones. Molecular docking on the interactions between OPFRs and OGT provided rationales for the difference in their structure-dependent inhibition potency. For the six OPFRs substituted with aromatic group or chlorinated alkyl chains, the calculated binding energy of the docked complexes follows the order TCrP > TPhP > EHDPP > TDCP > TCPP ≈ TCEP, with TCrP being the lowest (Table 1). This trend correlates very well with the experimentally measured inhibition potency (IC_{50}) of OPFRs. While, for the alkyl group substituted OPFRs, the existence of unfavorable interaction led to higher binding energy and completely ineffective inhibition potency. The results support the validity of the molecular docking approach.

In the cell based OGT activity assays, the inhibition effect of the six OPFRs substituted with aromatic group or chlorinated alkyl chains was further confirmed. The inhibition potency of aromatic group substituted OPFR, TCrP, is the strongest, which is in accordance with the results obtained from the electrochemical biosensor. However, the order of inhibition potency of other five OPFRs was not consistent with the results of the biosensor. The possible reason is that the situation of cell is more complicated as multiple factors, such as cell permeation, structure characteristics of OPFRs, as well as the interference of coexisting protein, may influence the inhibition reaction. Moreover, neither gene nor protein expression of OGT was restrained by OPFRs. This indicates that the decrease of OGT activity was indeed caused by the inhibition of OPFRs, rather than by the changes of OGT expression level.

Thereafter, we further investigated the subsequent biological effects derived from the inhibition. Intracellular O-GlcNAcylation is involved in essential cellular and physiological processes such as synaptic activity, neuronal morphogenesis, and learning and memory. Since OGT participates in the regulation of intracellular protein O-GlcNAcylation level by catalyzing the attachment of GlcNAc, inhibition of OGT activity should lead to a decrease in O-GlcNAc level in cells. We first found the reduced global O-GlcNAc level in whole cells. Then, we chose Nup62 and tau as two representative substrates of OGT to evaluate the effect of OGT inhibition in PC12 cells. As expected, the six OPFRs resulted in significant decrease of O-GlcNAcylated protein in PC12 cells. Nup62, a

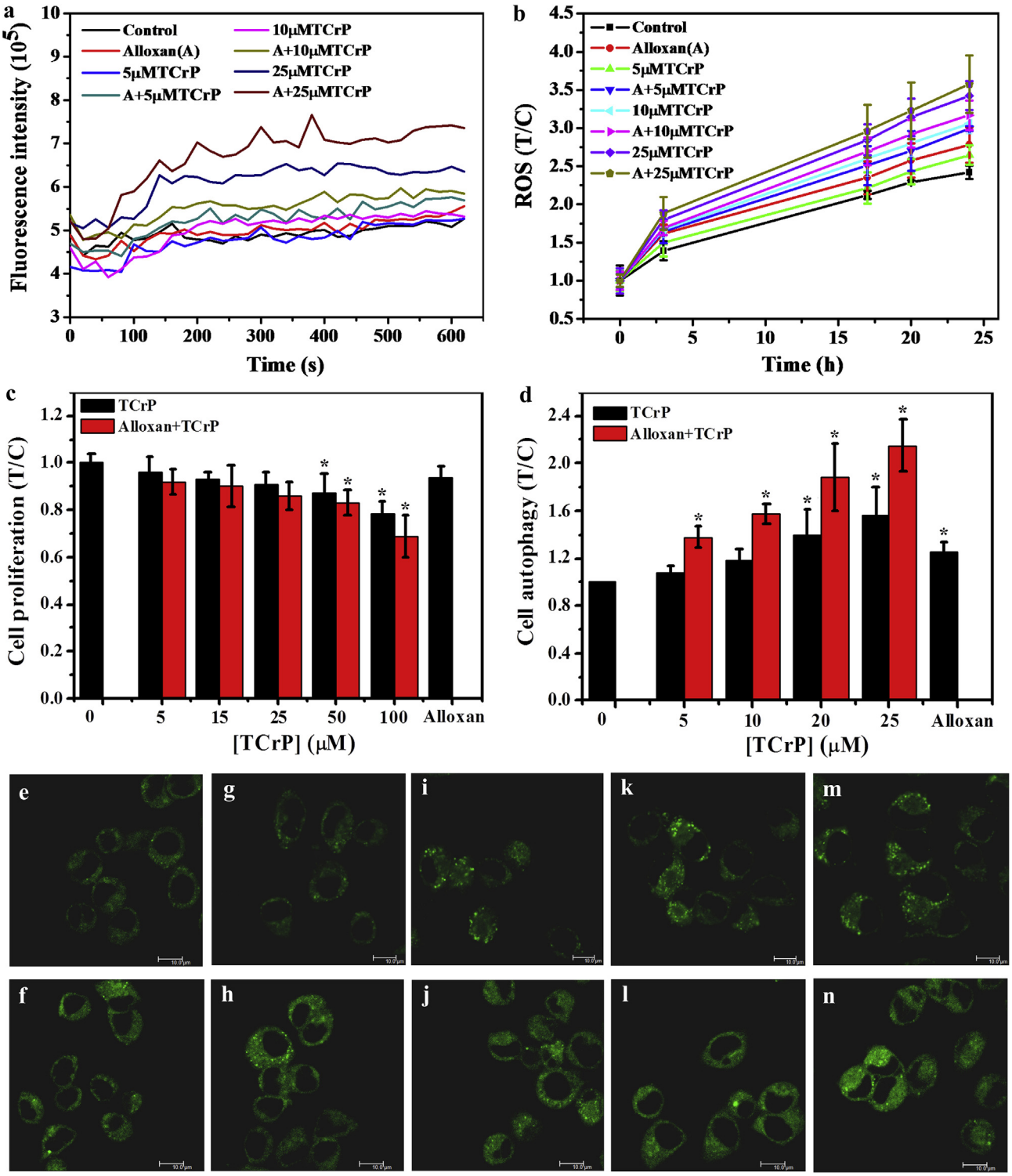

Fig. 6. The change of calcium ion level (a), ROS amounts (b), cell proliferation (c), cell autophagy (d) and confocal laser scanning microscope image in exposed cells to control medium (e), 5 mM alloxan (f), 5 μM TCrP (g), 5 mM alloxan and 5 μM TCrP (h), 10 μM TCrP (i), 5 mM alloxan and 10 μM TCrP (j), 20 μM TCrP (k), 5 mM alloxan and 20 μM TCrP (l), 25 μM TCrP (m), 5 mM alloxan and 25 μM TCrP (n).

main heavily glycosylated component of the nuclear pore, is a member of the FG-repeat containing nucleoporins and is localized to the nuclear pore central plug. This protein associates with the importin alpha/beta complex which is involved in the import of proteins containing nuclear localization signals [43]. Thus, changes in the level of O-GlcNAcylated Nup62 can affect the exchange and transmission of proteins between nucleus and cytoplasm. Tau is a microtubule-associated protein that serves to stabilize microtubules [44]. Changes in the level of tau O-GlcNAc modification has critical roles in controlling normal neuronal function, and modulating the pathological condition of neurodegenerative diseases such as AD. Similarly to other cytoplasmic proteins, tau undergoes O-GlcNAcylation at specific serine and threonine residues that can also be phosphorylated. Tau O-GlcNAcylation and phosphorylation are mutually exclusive, suggesting that an impaired O-GlcNAcylation might cause tau hyperphosphorylation and aggregation. Actually, many believe that hyperphosphorylation of the tau protein may

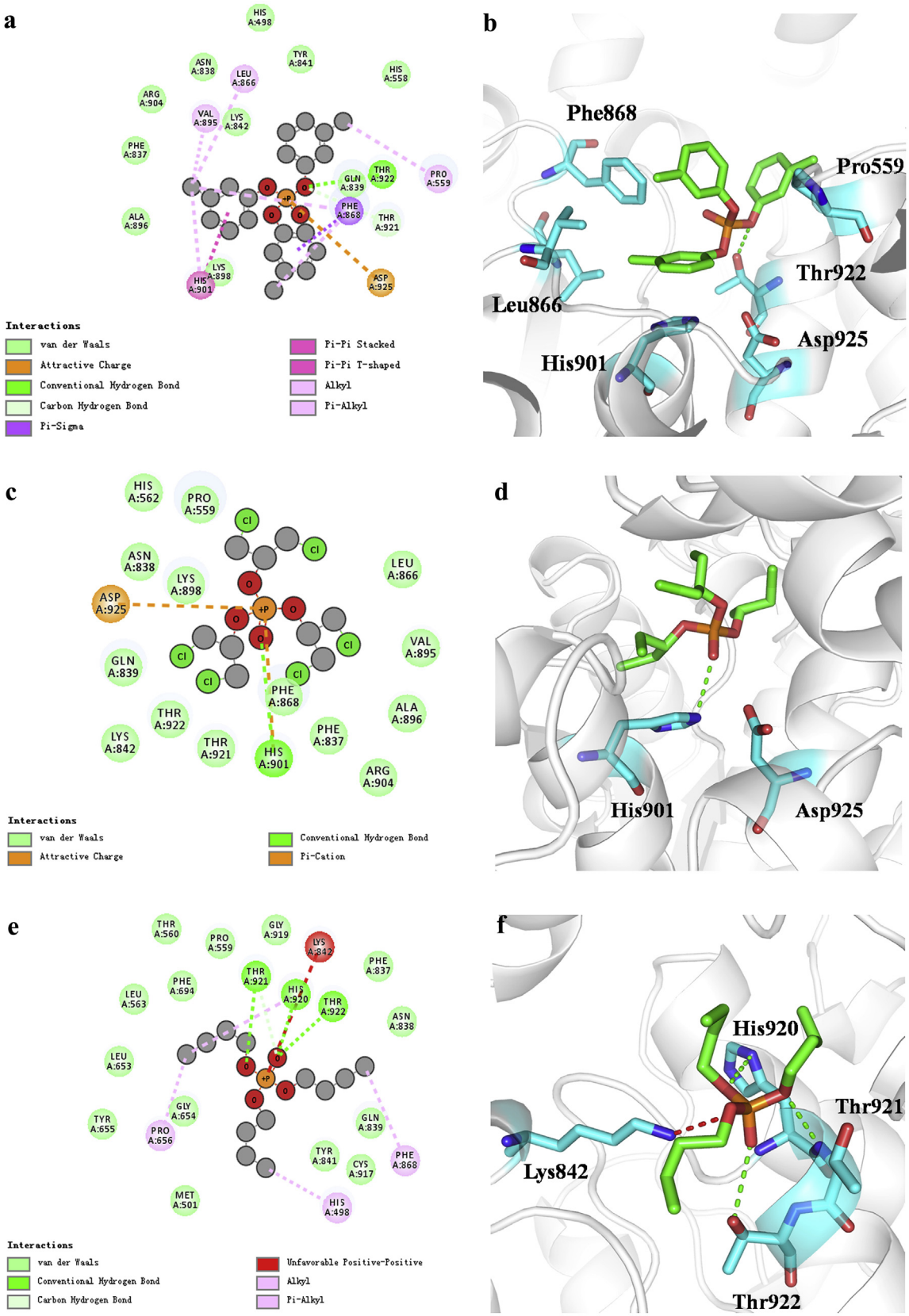

Fig. 7. Molecular model of aromatic, chlorinated alkyl or alkyl groups substituted OPFRs bound with OGT. The nonconvalent bonds formed between OGT and TCrP (a), TDCP (c), TnBP (e), respectively. For the compounds, carbon atoms are colored in gray, oxygen in red, phosphorus in orange, chlorine in green. Steric configuration for the docked complexes between OGT binding domain and TCrP (b), TDCP (d), TnBP (f), respectively. Hydrogen bonds are represented by dotted green lines. (For interpretation of the references to colour in this figure legend, the reader is referred to the web version of this article.)

be affected by its O-GlcNAcylation status [45]. If so, a reduction in tau O-GlcNAcylation might contribute to the pathophysiology of AD because hyperphosphorylated tau gives rise to neurofibrillary tangles, which are found in the AD brain and lie at the core of neurodegenerative processes associated with AD.

Besides, other biological effects including $[Ca^{2+}]_i$, ROS, cell proliferation and autophagy were also investigated. In the alloxan (an OGT inhibitor) exposed cells, we found the remarkable change of these biological effects, suggesting that OGT inhibition was capable of evoking these change. TCrP and alloxan coexposed cells could strengthen the extents of these change, indicating the pivotal role of TCrP in these effects. Based on the above findings that TCrP could inhibit the OGT activity in PC12 cells, we inferred that the variety caused by TCrP was at least in part mediated by the inhibition of OGT activity. Certainly, there are other unknown pathways induced by TCrP, resulting in the occurrence of these effects. Moreover, the abnormal change of above biological effects may pose health risk to the nerve system of the living organisms. A large body of evidence indicates that as a second messenger, cytosolic Ca^{2+} has important and diverse roles in the control of neuronal activity, axonal and dendritic growth and guidance, cognitive function, memory formation etc [46]. Excessive amounts of ROS can cause oxidative damage to lipids, proteins and DNA [47]. Signs of increased oxidative stress are apparent in the brain taken from patients with the neurodegenerative disorders AD and Parkinson's disease (PD), as well as other neurological diseases, with evidence in these diseases for protein modifications induced directly by ROS or indirectly by lipid peroxidation products [48]. Cell proliferation is the increase in cell number as a result of cell growth and division. Neuro cell can change the neuronal microenvironment by secreting neurotrophic factors and neurotransmitter. Once neuro cell proliferation was suppressed and subsequent cell numbers were decreased, it would affect the growth, development and biological function of nerve system. Also, mounting evidence has implicated autophagic dysfunction in the pathogenesis of several major neurodegenerative disorders, such as PD, AD and Huntington's disease [49]. Virtually, predictive targets (or biomarkers), especially those of early effect, would be of utmost value to predict and prevent the development of serious toxicity manifested in the human population.

The findings provided in our study probably illuminated the association between OPFRs exposure and its developmental neurotoxicity. It remains to be seen whether OGT inhibition by OPFRs would have any impacts on synaptic transmission and synaptic plasticity at cellular level.

In summary, by combining multiple experimental approachs including biosensor-based enzyme activity assay, cell-based assays and molecular docking, we have established OGT as a new cellular target of OPFRs. In a cellular system, six different forms of OPFRs, substituted with aromatic or chlorinated alkyl group, preferentially target OGT, and inhibit the OGT activity, and thereby suppress intracellular protein O-GlcNAc modification, and subsequently lead to some deleterious biological effects. The new target OGT may provide a clue to *in vivo* toxic effects of OPFRs. Further studies are needed to investigate the effects of OGT inhibition on synaptic transmission and synaptic plasticity and its possible link to the toxic effects observed on experimental animals.

Acknowledgments

This work was supported by the National Natural Science Foundation of China (No. 21377142, 21577163, 21375143, 21477146, 21621064, 91543203) and Chinese Academy of Sciences (XDB14040100, QYZDJ-SSW-DQC020)

Conflict of interest

None of the authors have any conflict of interest to declare.

References

[1] I. Van der Veen, J. De Boer, Phosphorus flame retardants: properties, production, environmental occurrence, toxicity and analysis, Chemosphere 88 (2012) 1119–1153.
[2] G.L. Wei, D.Q. Li, M.N. Zhuo, Y.S. Liao, Z.Y. Xie, T.L. Guo, J.J. Li, S.Y. Zhang, Z.Q. Liang, Organophosphorus flame retardants and plasticizers: sources, occurrence, toxicity and human exposure, Environ. Pollut. 196 (2015) 29–46.
[3] T. Reemtsma, J.B. Quintana, R. Rodil, M. Garcia-LOPFRz, I. Rodriguez, Organophosphorus flame retardants and plasticizers in water and air I. Occurrence and fate, TRAC-Trends Anal. Chem. 27 (2008) 727–737.
[4] N. Van den Eede, A.C. Dirtu, H. Neels, A. Covaci, Analytical developments and preliminary assessment of human exposure to organophosphate flame retardants from indoor dust, Environ. Int. 37 (2011) 454–461.
[5] W.N. Wan, S.Z. Zhang, H.L. Huang, T. Wu, Occurrence and distribution of organophosphorus esters in soils and wheat plants in a plastic waste treatment area in China, Environ. Pollut. 214 (2016) 349–353.
[6] U.E. Bollmann, A. Moler, Z.Y. Xie, R. Ebinghaus, J.W. Einax, Occurrence and fate of organophosphorus flame retardants and plasticizers in coastal and marine surface waters, Water Res. 46 (2012) 531–538.
[7] S.X. Cao, X.Y. Zeng, H. Song, H.R. Li, Z.Q. Yu, G.Y. Sheng, J.M. Fu, Levels and distributions of organophosphate flame retardants and plasticizers in sediment from Taihu Lake, China, Environ. Toxicol. Chem. 31 (2012) 1478–1484.
[8] K. Hoffman, C.M. Butt, A. Chen, A.T. Limkakeng, H.M. Stapleton, High exposure to organophosphate flame retardants in infants: associations with baby products, Environ. Sci. Technol. 49 (24) (2015) 14554–14559.
[9] J.W. Kim, T. Isobe, M. Muto, N.M. Tue, K. Katsura, G. Malarvannan, A. Sudaryanto, K.H. Chang, M. Prudente, P.H. Viet, Organophosphorus flame retardants (PFRs) in human breast milk from several Asian countries, Chemosphere 116 (2014) 91–97.
[10] K. Hoffman, S. Garantziotis, L.S. Birnbaum, H.M. Stapleton, Monitoring indoor exposure to organophosphate flame retardants: hand wipes and house dust, Environ. Health Persp. 123 (2015) 160–165.
[11] L.V. Dishaw, C.M. Powers, I.T. Ryde, S.C. Roberts, F.J. Seidler, T.A. Slotkin, H.M. Stapleton, Is the PentaBDE replacement, tris (1,3-dichloro-2-propyl) phosphate (TDCPP), a developmental neurotoxicant? Studies in PC12 cells, Toxicol. Appl. Pharm. 256 (2011) 281–289.
[12] Q.W. Wang, J.C.W. Lam, Y.C. Man, N.L.S. Lai, K.Y. Kwok, Y.Y. Guo, P.K.S. Lam, B.S. Zhou, Bioconcentration, metabolism and neurotoxicity of the organophorous flame retardant 1,3-dichloro 2-propyl phosphate (TDCPP) to zebrafish, Aquat. Toxicol. 158 (2015) 108–115.
[13] A.V. Terry, Functional consequences of repeated organophosphate exposure: potential non-cholinergic mechanisms, Pharmacol. Therapeu. 134 (2012) 355–365.
[14] National Toxicology Program. NTP toxicology and carcinogenesis studies of tris (2-chloroethyl) phosphate (CAS No. 115-96-8) in F344/N rats and B6C3F1 mice (gavage studies). National Toxicology Program technical report series, 1991, 391, 1–18.
[15] M. Lotti, A. Moretto, Organophosphate-induced delayed polyneuropathy, Toxicol. Rev. 24 (2005) 37–49.
[16] M.B. Abou-Donia, Organophosphorus ester-induced chronic neurotoxicity, Arch. Environ. Health 58 (2003) 484–497.
[17] D.J. Read, Y. Li, M.V. Chao, J.B. Cavanagh, P. Glynn, Neuropathy target esterase is required for adult vertebrate axon maintenance, J. Neurosci. 29 (2009) 11594–11600.
[18] W.Y. Hou, D.X. Long, H.P. Wang, Q. Wang, Y.J. Wu, The homeostasis of phosphatidylcholine and lysophosphatidylcholine was not disrupted during tri-o-cresyl phosphate-induced delayed neurotoxicity in hens, Toxicology 252 (2008) 56–63.
[19] L.L. Yuan, J.S. Li, J.M. Zha, Z.J. Wang, Targeting neurotrophic factors and their receptors, but not cholinesterase or neurotransmitter, in the neurotoxicity of TDCPP in Chinese rare minnow adults (Gobiocypris rarus), Environ. Pollut. 208 (2016) 670–677.
[20] N. Ta, C.N. Li, Y.J. Fang, H.L. Liu, B.C. Lin, H. Jin, L. Tian, H.S. Zhang, W. Zhang, Z.G. Xi, Toxicity of TDCPP and TCEP on PC12 cell: changes in CAMKII, GAP43, tubulin and NF-H gene and protein levels, Toxicol. Lett. 227 (2014) 164–171.
[21] S.F. Wang, B. Wan, L.Y. Zhang, Y. Yang, L.H. Guo, *In vitro* inhibition of lysine decarboxylase activity by organophosphate esters, Biochem. Pharmacol. 92 (2014) 506–516.
[22] T.M. Gloster, Advances in understanding glycosyltransferases from a structural perspective, Curr. Opin. Struct. Biol. 28 (2014) 131–141.
[23] Z.G. Levine, S. Walker, The biochemistry of O-GlcNAc transferase: which functions make it essential in mammalian cells? Annu. Rev. Biochem. 85 (2016) 631–657.
[24] J.C. Trinidad, D.T. Barkan, B.F. Gulledge, A. Thalhammer, A. Sali, R. Schoepfer, A.L. Burlingame, Global identification and characterization of both O-GlcNAcylation and phosphorylation at the murine synapse, Mol. Cell. Proteomics 11 (2012) 215–229.
[25] Y. Akimoto, F.I. Comer, R.N. Cole, A. Kudo, H. Kawakami, H. Hirano, G.W. Hart, Localization of the O-GlcNAc transferase and O-GlcNAc-modified proteins in rat cerebellar cortex, Brain Res. 966 (2003) 194–205.
[26] R.N. Cole, G.W. Hart, Cytosolic O-glycosylation is abundant in nerve terminals, J. Neurochem. 79 (5) (2001) 1080–1089.
[27] M. Yanagisawa, R.K. Yu, O-Linked beta-N-Acetylglucosaminylation in mouse embryonic neural precursor cells, J. Neurosci. Res. 87 (2009) 3535–3545.
[28] Y.P. Zhu, X.Y. Shan, S.A. Yuzwa, D.J. Vocadlo, The emerging link between O-GlcNAc and Alzheimer disease, J. Biol. Chem. 289 (2014) 34472–34481.
[29] P.S. Banerjee, O. Lagerlof, G.W. Hart, Roles of O-GlcNAc in chronic diseases of aging, Mol. Aspects Med. 51 (2016) 1–15.

[30] C. Mizuguchi-Hata, Y. Ogawa, M. Oka, Y. Yoneda, Quantitative regulation of nuclear pore complex proteins by O-GlcNAcylation, BBA-Mol. Cell Res. 1833 (2013) 2682–2689.
[31] N. O'Donnell, N.E. Zachara, G.W. Hart, J.D. Marth, Ogt-dependent X-chromosome-linked protein glycosylation is a requisite modification in somatic cell function and embryo viability, Mol. Cell. Biol. 24 (2004) 1680–1690.
[32] A.C. Wang, E.H. Jensen, J.E. Rexach, H.V. Vinters, L.C. Hsieh-Wilson, Loss of O-GlcNAc glycosylation in forebrain excitatory neurons induces neurodegeneration, Proc. Natl. Acad. Sci. 113 (2016) 15120–15125.
[33] C. Su, T.L. Schwarz, O-GlcNAc transferase is essential for sensory neuron survival and maintenance, J. Neurosci. 37 (2017) 2125–2136.
[34] A.P. Willems, M. Gundogdu, M.J.E. Kempers, J.C. Giltay, R. Pfundt, M. Elferink, B.F. Loza, J. Fuijkschot, A.T. Ferenbach, K.L.I. van Gassen, Mutations in N-acetylglucosamine (O-GlcNAc) transferase in patients with X-linked intellectual disability, J. Biol. Chem. 292 (2017) 12621–12631.
[35] T.W. Hamann, F. Gstrein, B.S. Brunschwig, N.S. Lewis, Measurement of the free-energy dependence of interfacial charge-transfer rate constants using ZnO/H_2O semiconductor/liquid contacts, J. Am. Chem. Soc. 127 (2005) 7815–7824.
[36] Y. Yang, Y.X. Gu, B. Wan, X.M. Ren, L.H. Guo, Label-free electrochemical biosensing of small-molecule inhibition on O-GlcNAc glycosylation, Biosens. Bioelectron. 95 (2017) 94–99.
[37] K. Kerman, M. Vestergaard, E. Tamiya, Label-free electrical sensing of small-molecule inhibition on tyrosine phosphorylation, Anal. Chem. 79 (2007) 6881–6885.
[38] Y. Wang, J.J. Zhu, L.W. Zhang, Discovery of cell-permeable O-GlcNAc transferase inhibitors via tethering in situ click chemistry, J. Med. Chem. 60 (2017) 263–272.
[39] J.J.P. Stewart, MOPAC: a semiempirical molecular-orbital program, J. Comput. Aided Mol. Des. 4 (1990) 1–45.
[40] D. Van der Spoel, E. Lindahl, B. Hess, G. Groenhof, A.E. Mark, H.J.C. Berendsen, GROMACS: fast, flexible, and free, J. Comput. Chem. 26 (2005) 1701–1718.
[41] M.B. Lazarus, Y.S. Nam, J.Y. Jiang, P. Sliz, S. Walker, Structure of human O-GlcNAc transferase and its complex with a peptide substrate, Nature 469 (2011) 564–569.
[42] H.C. Dorfmueller, V.S. Borodkin, D.E. Blair, S. Pathak, I. Navratilova, D.M.F. Van Aalten, Substrate and product analogues as human O-GlcNAc transferase inhibitors, Amino Acids 40 (2011) 781–792.
[43] G.D. Holt, C.M. Snow, A. Senior, R.S. Haltiwanger, L. Gerace, G.W. Hart, Nuclear pore complex glycoproteins contain cytoplasmically disposed O-linked N-acetylglucosamine, J. Cell Biol. 104 (1987) 1157–1164.
[44] C.S. Arnold, G.V.W. Johnson, R.N. Cole, D.L.Y. Dong, M. Lee, G.W. Hart, The microtubule-associated protein tau is extensively modified with O-linked N-acetylglucosamine, J. Biol. Chem. 271 (1996) 28741–28744.
[45] C.X. Gong, F. Liu, K. Iqbal, O-GlcNAcylation: a regulator of tau pathology and neurodegeneration, Alzheimers Dement. 12 (2016) 1078–1089.
[46] M.J. Berridge, P. Lipp, M.D. Bootman, The versatility and universality of calcium signalling, Nat. Rev. Mol. Cell Biol. 1 (2000) 11–21.
[47] P. Poprac, K. Jomova, M. Simunkova, V. Kollar, C.J. Rhodes, M. Valko, Targeting free radicals in oxidative stress-related human diseases, Trends Pharmacol. Sci. 38 (2017) 592–607.
[48] G. Perry, A.K. Raina, A. Nunomura, T. Wataya, L.M. Sayre, M.A. Smith, How important is oxidative damage? Lessons from Alzheimer's disease, Free Radical Biol. Med. 28 (2000) 831–834.
[49] I. Benito-Cuesta, H. Diez, L. Ordonez, F. Wandosell, Assessment of autophagy in neurons and brain tissue, Cells (2017), http://dx.doi.org/10.3390/cells6030025.